Experimental validation of a model for the response function of Chirp-Pulse Microwave Computerized Tomography (CP-MCT)

M. Miyakawa, K. Orikasa

Department of Biocybernetics, Faculty of Engineering, Niigata University, 8050 Ikarashi2, Niigata 950-2181, Japan

M. Bertero, P. Boccacci

INFM and DISI, Universita' di Genova, Via Dodecaneso 35, I-16146 Genova, Italy

F. Conte, M. Piana

INFM and DIFI, Universita' di Genova, Via Dodecaneso 33, I-16146 Genova, Italy

Abstract. In this paper we develop a method for the experimental determination of the response function in CP-MCT and we compare the result with that obtained from a theoretical model proposed in a previous paper. We find a satisfactory agreement. In addition we develop a method for computing the response function of a pixel with arbitrary location.

1. Introduction

Microwave Tomography (MT) is a low-resolution high-contrast imaging modality. Operating at 1 GHz, which corresponds to a few centimeters wavelength in biological tissues, provides a spatial resolution of the order of 1 cm, which is very poor if compared to the millimeter spatial resolution accomplished by X-rays or ultrasounds. On the other hand, sensitivity optimum frequency range for biological tissues is located just between 1 and 3 GHz, which allows 20 to 30 cm investigation depth. This efficiency in pointing out weak contrasts make MT worthwhile investigation. According to a very general approach MT aims to retrieve maps of the complex refractive index from measurements of the diffracted electromagnetic field. However here we will deal with a very specific MT technique, particularly helpful in non-invasive termometry, which allows the restoration of temperature-related attenuation constants. In general the dependence of complex permittivity to temperature is extremely complicated and is

influenced by many parameters such as the incident wave frequency or the tissue composition and pathologies.

Diffraction effects at the origin of the MT spatial resolution coarseness also affect the image processing task. In fact the inverse problem of providing microwave images from near- or far-field patterns is strongly complicated by two mathematical pathologies both related to the significant scattering effects occuring during the microwave beam - biological target interaction. First the imaging problem is severely ill-conditioned so that a dramatic numerical instability must be faced at some stage of the processing. Second, the reconstruction problem is strongly non-linear and this makes the application of regularization techniques for reducing numerical instabilities computationally heavy.

There are two main trends in addressing these two difficulties. The first approach is to considering the diffraction effects in their own complexity and to performing the restoration by means of non-linear optimization schemes. This method is in general extremely accurate but typically requires a strong computational effort since these iterative algorithms involve the solution of the corresponding direct problem at each step of the procedure. The second approach, which is the one considered in the present paper, aims to reproduce an X-ray situation where the contribution of the straight path joining the source antenna to the receiver one is isolated by means of a specific technique named Microwave Time Delay Spectroscopy (MTDS) [3].

This paper is the third one of a series of papers [4, 5] devoted to providing a linear modelization of data acquisition in Chirp-Pulse Microwave Computerized Tomography (CP-MCT). This is a technique which has been designed for imaging temperature variations inside a body, via temperature dependence of the attenuation and/or phase constant of the microwaves [1, 2]. In the Department of Biocybernetics at Niigata University a CP-MCT prototype has been developed, whose geometry is precisely that of the first-generation X-ray tomographic scanners: two microwave antennas, one transmitting, the source S, and one receiving, the receiver R, are moved along two parallel lines which define the plane to be imaged; then the system is rotated by a certain angle and the scanning operation is repeated; the system is rotated again and so on up to cover the angle π. In the prototype fifty equispaced directions are used. The source emits an electromagnetic field whose time dependence is described by a chirp signal with frequency range (ω_1, ω_2) and sweep time T_S

$$c(t) = A\chi(t)\sin(\omega_1 t + \frac{1}{2}Kt^2) \quad , \tag{1.1}$$

$\chi(t)$ being the characteristic function of the interval $(0, T_S)$ and

$$K = \frac{\omega_2 - \omega_1}{T_S} \quad . \tag{1.2}$$

For each position of the source-receiver pair MTDS is used to extract from the received signal the contribution of the straight path joining the two antennas: part of the input

signal is multiplied by the output field by means of the mixer; since the frequency of the beating term in the mixed signal depends on the delay time with which the contributions from the various paths reach the receiver, the straight line contribution is selected by means of a Band Pass Filter; finally, the basic algorithm of X-ray tomography, the Filtered Back Projection (FBP), is used for obtaining a map of the attenuation and/or phase constant variations, hence of the temperature variations across the body.

The main features of our linear model are:

- The model is 2-D and therefore it is particularly suitable to describing experimental situations where cylindrical simmetry can be reliably assumed. However the generalization to three dimensions is straightforward.
- TM polarization is assumed (i.e., electric field parallel to the direction of the antenna). The extension to TE mode (i.e., magnetic field parallel to the direction of the antenna) is conceptually straightforward, though the boundary value problem involved in the data acquisition description would be more complicated.
- A generic body under investigation is approximated by a set of small pixels; the projection of the body, i.e. the values of the electric field at the exit of the filter, as a function of the position of the antennas and for a fixed rotation angle, is approximated by a linear combination of the projections of the characteristic function of the pixels. The coefficients of the linear combination are proportional to the attenuation constant of the corresponding pixels. The projection of the characteristic function of each pixel is obtained by solving the Lippmann-Schwinger equation under Born approximation assumptions.

In paper [5] this linear model is firstly formulated and some preliminary computations for its validation are performed. In particular, it is shown that the shape of the response function for a pixel located in the center of the scanner at Niigata does not strongly depend on the relative contrast between the pixel and the bolus and that the area of the response function is roughly proportional to the relative contrast. However a systematic validation of the model is addressed in the present paper. In particular in Section 2 the model for the response function is described and the projection for a general position of the S-R pair and for a general rotation angle is computed by exploiting some simmetry relationships between the projection of differently located pixels. In Section 3 CP-MCT projections are computed for a few pixels located at different distances from the centre. The results of this simulation encourage to assess that the PSF of our scanner can be assumed as substantially space invariant and furthermore that an improvement in resolution occurs for points at the boundary of the observation region. Then in Section 4 and Section 5 an experimental method for the computation of the PSF is described. The results of this approach, based on a regularized multiple deconvolution of real data corresponding to cylindrical phantoms with different radius, are compared to the ones obtained by means of our linear model.

Finally we point out that the reliability of the model naturally inspires an approach to CP-MCT imaging more sophisticated and hopefully more effective than the simple application of FBP. The description of this approach and its application in the case of real data registered by Niigata prototype will be treated in a future paper entirely devoted to the image restoration inverse problem.

2. The model of the response function

In [5] a 2D model of CP-MCT is considered, by assuming that both the source and the receiver can be represented by linear antennas orthogonal to the plane to be imaged. The intersections of the antennas with the plane are denoted by $\mathbf{x}_S$ and $\mathbf{x}_R$ respectively. The distance between the two antennas is d and is kept fixed when the two antennas are moved along the direction $\theta = (cos\phi, sin\phi)$, orthogonal to the line from $\mathbf{x}_S$ to $\mathbf{x}_R$ (see Figure 1). The direction of the latter is denoted by $\theta^{\perp} = (-sin\phi, cos\phi)$.

The source emits a TM electromagnetic field (electric field parallel to the direction of the antenna) whose time dependence is described by a chirp signal with frequency range (ω_1, ω_2) and sweep-time T_S

$$c(t) = A\chi(t)\sin(\omega_1 t + \frac{1}{2}Kt^2), \tag{2.1}$$

$\chi(t)$ being the characteristic function of the interval $(0, T_S)$ and

$$K = \frac{\omega_2 - \omega_1}{T_S}. \tag{2.2}$$

In addition, in order to model the response function of a pixel at $\mathbf{x}_P$, we consider a cylindrical phantom with a small diameter, also orthogonal to the plane, whose intersection with the plane is just $\mathbf{x}_P$. We assume that the phantom is immersed in a homogeneous absorbing medium (the bolus) and we denote by ϵ_P, σ_P the electrical parameters of the phantom (relative dielectric constant and electrical conductivity) and by ϵ_b, σ_b those of the bolus. The corresponding attenuation constants are denoted by α_P and α_b, while the relative contrast between the attenuation constants is defined by

$$\gamma = \frac{\alpha_P - \alpha_b}{\alpha_b}. \tag{2.3}$$

In [5] we prove that, if $\mathbf{x}_P$ is not too close to $\mathbf{x}_R$ or $\mathbf{x}_S$, then the Fourier transform of the field received in $\mathbf{x}_R$ is given by

$$\hat{u}(\mathbf{x}_R, \mathbf{x}_S; \omega) \simeq \frac{i}{4}\hat{c}(\omega)\left\{\sqrt{\frac{2}{\pi}}e^{-i\pi/4}\frac{e^{ik_b d}}{\sqrt{k_b d}} - \right. \tag{2.4}$$

$$\left. -\frac{1}{2}(ak_0)^2 m_P \frac{e^{ik_b(|\mathbf{x}_P - \mathbf{x}_S| + |\mathbf{x}_P - \mathbf{x}_R|)}}{k_b\sqrt{|\mathbf{x}_P - \mathbf{x}_S||\mathbf{x}_P - \mathbf{x}_R|}}\right\}$$

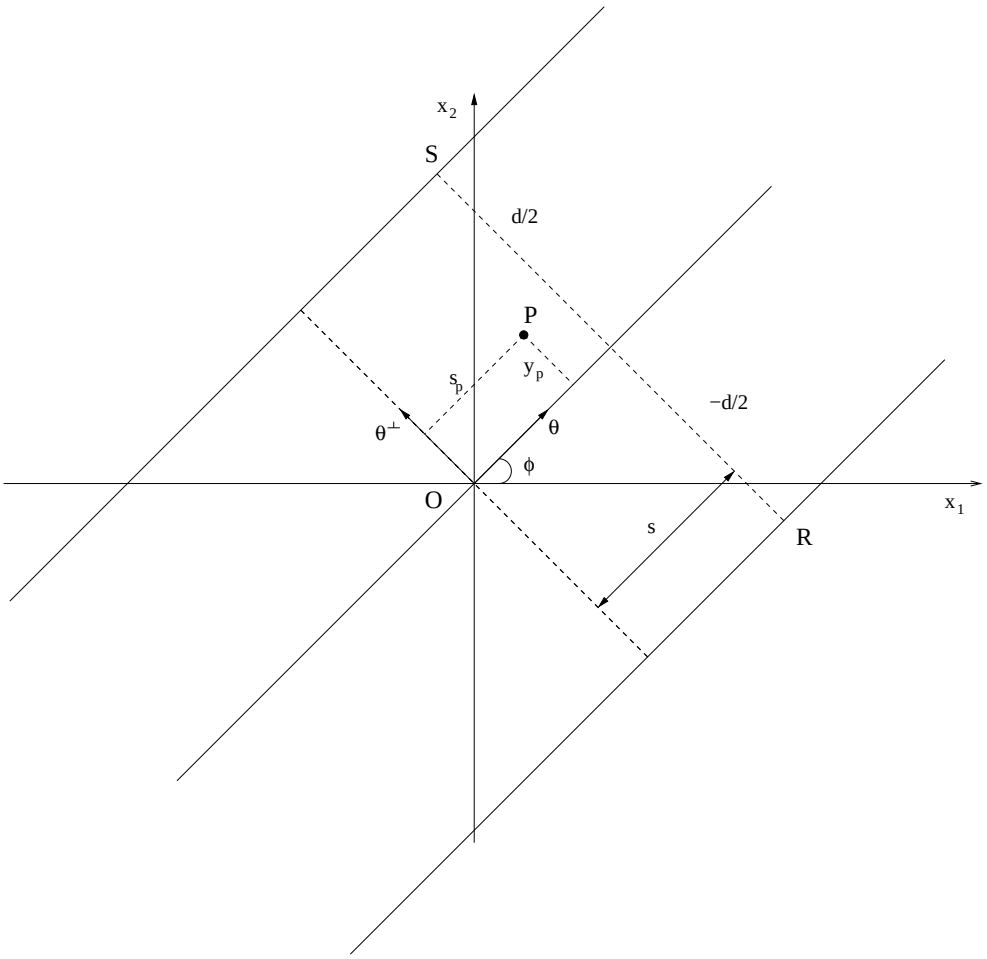

Figure 1. Scheme of the scanning geometry in CP-MCT. The points S, R and P correspond to source, receiver and phantom, respectively. The coordinates with respect to the system defined by the pair of vectors $\theta, \theta^{\perp}$ are also indicated.

where $\hat{c}(\omega)$ denotes the Fourier transform of $c(t)$ and

$$m_P = \epsilon_b - \epsilon_P + i\frac{\sigma_b - \sigma_P}{\epsilon_0 \omega}. \tag{2.5}$$

For a given position of the S-R pair the datum provided by CP-MCT can be computed as follows:

- compute the convolution product of $\hat{u}(\mathbf{x}_R, \mathbf{x}_S; \omega)$ with $\hat{c}(\omega)$

$$\hat{s}_M(\mathbf{x}_R, \mathbf{x}_S; \omega) = \frac{1}{2\pi}(\hat{c} * \hat{u})(\mathbf{x}_R, \mathbf{x}_S; \omega); \tag{2.6}$$

- compute the maximum value of the modulus of $\hat{s}_M(\mathbf{x}_R, \mathbf{x}; \omega)$;

- subtract the constant term due to the bolus (the background);
- take the logarithm of the result.

For fixed θ, the result of the last step, as a function of the position s of the S-R pair provides the CP-MCT *projection*, in the direction θ, of the phantom. The set of all projections is a function of two variables which can be called the CP-MCT *transform* of the phantom.

As we see from equation (2.4), this transform depends on the distances phantom-source and phantom-receiver, i.e. $r_{P,S} = |\mathbf{x}_P - \mathbf{x}_S|$ and $r_{P,R} = |\mathbf{x}_P - \mathbf{x}_R|$ respectively, and is symmetric with respect to the exchange of these quantities. These properties imply several relationships between the projections of different phantoms. In order to exploit this point it is convenient to give the positions of source, receiver and phantom in terms of the coordinates defined by the unit vectors θ and $\theta^\perp$. We have (see Figure 1): $\mathbf{x}_S = (s, d/2)$, $\mathbf{x}_R = (s, -d/2)$, $\mathbf{x}_P = (s_P, d_P)$, so that

$$r_{P,S} = \sqrt{(s - s_P)^2 + (d_P - \frac{1}{2}d)^2} \tag{2.7}$$

$$r_{P,R} = \sqrt{(s - s_P)^2 + (d_P + \frac{1}{2}d)^2}. \tag{2.8}$$

We find that, for all phantoms with positions corresponding to a given value of d_P, the projections are obtained by translating that of the phantom with $s_P = 0$. In addition, for a given value of s_P, the phantoms corresponding to d_P and $-d_P$ have the same projections. It follows that the projections of all phantoms in all directions can be computed by computing the projections in the direction $\theta = (0, 1)$ of the phantoms with $s_P = 0$ and $d_P \geq 0$ (see Figure 2).

More precisely, if we denote by $P(s, d_P)$ the projection in the direction $(0, 1)$ of a phantom located in the point $(d_P, 0)$, then the projection in the direction θ of the same phantom located in the point $\mathbf{x}_P$ is given by

$$P_\theta(s) = P(s - s_P, |d_P|), \tag{2.9}$$

where s_P, d_P are the coordinates of the point $\mathbf{x}_P$ in the system defined by the pair of unit vectors θ,$\theta^\perp$.

In [5] we performed computations of $P(s, 0)$ for various values of the contrast defined in equation 2.3 and we found that the shape of the function does not strongly depend on γ while its area is roughly proportional to γ. Therefore the function $P(s, 0)$, computed for a moderate value of the contrast (for instance 30%), and normalized to unit area, can be taken as the response function of the central pixel. We investigate now what happens in the case of a phantom not located in the centre of the observation region.

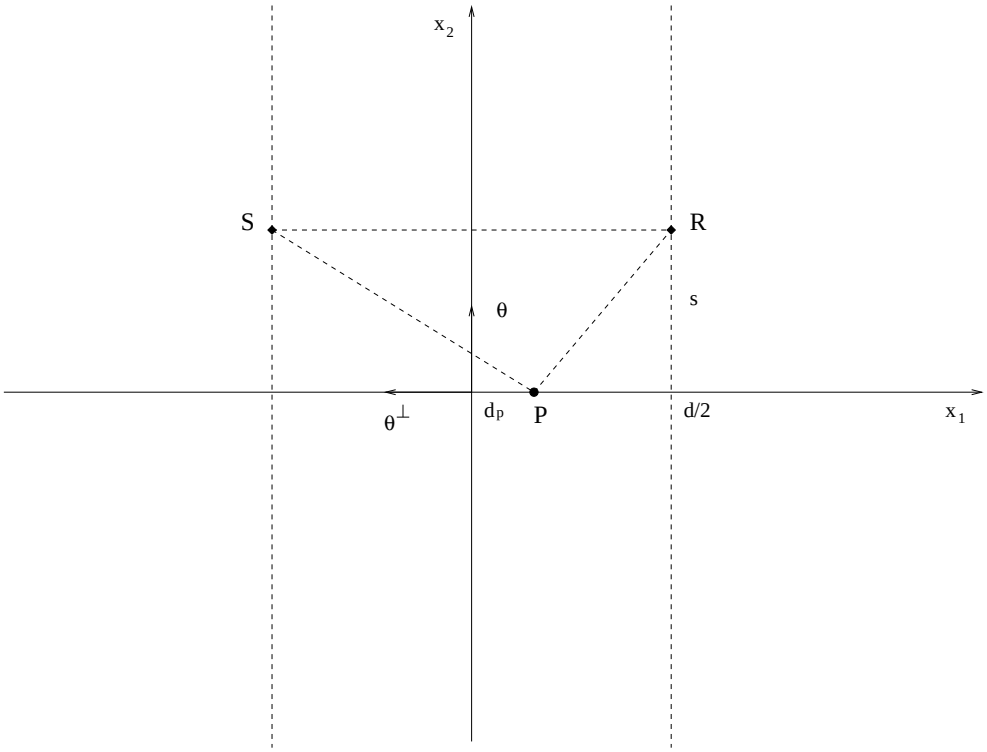

Figure 2. The simplified geometrical configuration which can be used for computing all projections of any phantom.

3. A numerical example

We have performed computations of the function $P(s, d_P)$ in cases which are significant for the prototype of CP-MCT scanner developed at Niigata University. Therefore, as concerns the features of the scanning system, we assume that the distance between the two antennas is 282 mm, because this is the value used in the prototype, and that the transmitting antenna is supplied with a chirp signal with frequency range from 1 to 2 GHz and sweep time of 200 ms.

As concerns the bolus and the phantom, in a first example we assume that the bolus is characterized by relative electrical permittivity equal to 73.89 and electrical conductivity equal to 1.78 Sm^{-1} (namely the values at 1.5 GHz for a saline solution with 0.69% concentration and temperature 32 $^{\circ}C$) while the phantom is characterized by relative electrical permittivity equal to 74.55 and electrical conductivity equal to 1.19 Sm^{-1} (the values at 1.5 GHz for a saline solution with 0.44% concentration and

temperature 32 $°C$). The bolus is more absorbing than the phantom and the contrast in the attenuation constant is about 33%.

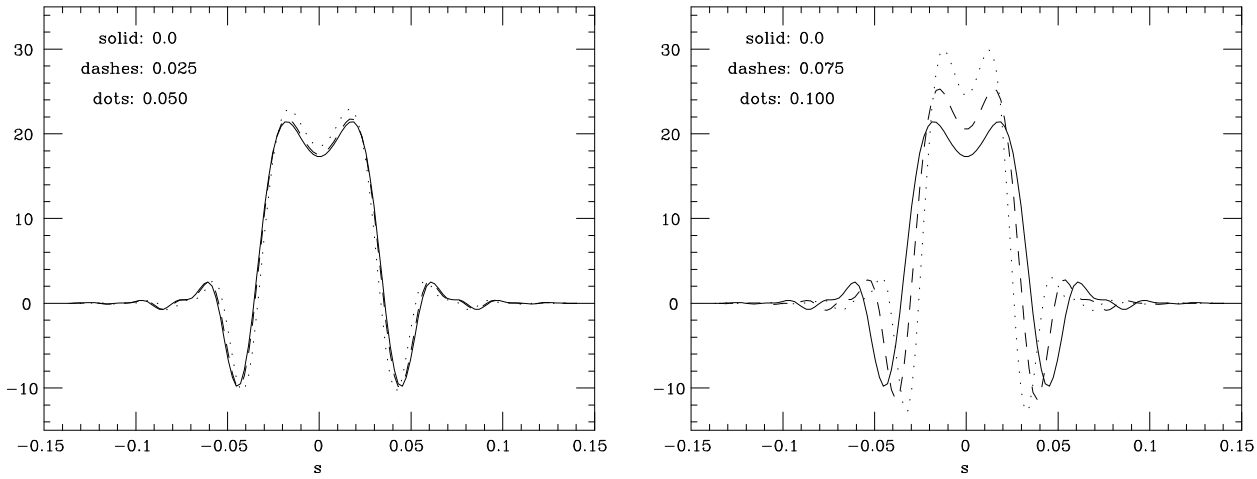

(a) (b)

Figure 3. Plot of the response functions corresponding to different distances from the centre: a) $d_P = 0, 0.025, 0.050m$; $d_P = 0, 0.075, 0.100m$.

A first important result of our computations is that, after background subtraction, the integrals of the projections do not depend significantly on the distance d_P of the phantom from the origin. Therefore these projections can be normalized in such a way that their integral is one. This is the normalization used for plotting our results which are given in Figure 3. These results are in agreement with those obtained by means of a code based on the FD-TD method [6, 7, 8].

A very interesting feature shown by these results is that the width of the central lobe decreases when d_P increases. This means that the resolution of CP-MCT imaging in points close to the boundary of the observation region is better than in points close to the centre, an effect which was observed experimentally. In addition the variations of the projections for points close to the centre are very slow and this property justifies the assumption of space invariance usedin [4].

4. The experimental approach

In principle the response function of a pixel, for instance the central one, can be measured by locating a cylinder with a small diameter in the centre of the scanning system and measuring its projections in the CP-MCT sense. Such an approach, however, is not feasibble in practice because, for a small cylinder, the signal-to-noise ratio is too low.

In order to get through this difficulty in [4] we proposed the following approach: measure the projection of a cylinder with a sufficiently large diameter and assume that the CP-MCT projection is the convolution product of the Radon projection with the response function of the central pixel. Of course such an approach assumes that the response function is not strongly space-variant but, as we already remarked, the results of the previous Section show that such an approximation is not too bad at least for regions close to the centre of the scanning system. It follows that the response function can be estimated by solving a deconvlution problem.

The results obtained in [4] by such an approach are not in a satisfactory agreement with the theoretical results obtained in [5]. More precisely the central lobe of the response function estimated in [4] does not have the typical structure, similar to a pair of horns, shown in Figure 3. As already discussed in [4], data provided by only one cylinder do not carry sufficient information about certain spatial frequencies related to the diameter of the cylinder. These lack of information can be the source of the disagreement. Therefore a quite natural extension of the approach proposed in [4] can consist in using data from several cylinders: the lack of information in the projection of one cylinder can be compensated by the information provided by the projection of another cylinder and vicecersa.

To this purpose measurements have been performed with the prototype at Niigata University for three cylinders with diameters respectively of $40, 60$ and 80 mm. The phantoms contain a saline solutions with concentration 0.44% while the bolus is a saline solution with concentration 0.69%. The temperature is $32\ ^{\circ}C$. These are precisely the values considered in the numerical example of the previous Section.

As in [4] for each cylinder we measured 50 projections corresponding to 50 equispaced angles between zero and π. The number of points is 256 per projection. Indeed oversampling is intentionally utilized to compensate for instabilities of the experimental setup. Since the size of each projection coincide with the distance between the two antennas, namely 282 mm, the sampling distance is 1.1 mm.

All projections have been processed as in [4] by subtracting the background and suppressing the out-of-band noise. A further processing is required for the following reason. Due to the symmetry of the phantom and of the instrument, all projections of a centred cylinder should be equal and symmetric with respect to the centre of the projection (except for noise contribution). These properties are not satisfied as a

consequence of various kinds of experimental errors, even if the variations from one projection to the other are not very large. Since these variations are not systematic, we process the data in order to get a projection having the good properties. The processing consists in taking the average of all projections and in symmetrizing the result. The projections of the three cylinders obtained in such a way are shown in Figure 4.

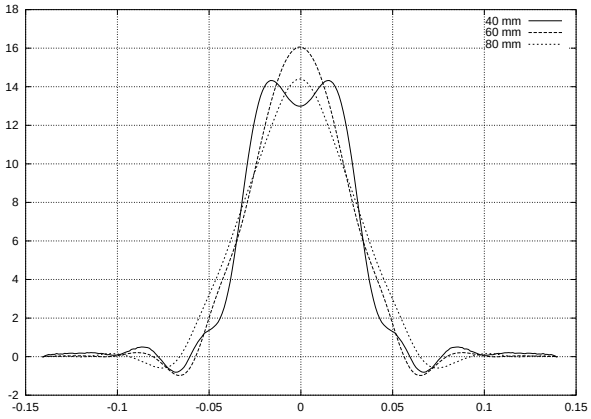

Figure 4. Projections of three cylinders with different diameters: 40 mm (dotted line), 60 mm (dashed line), 80 mm (full line).

An interesting feature of these results is that, in the case of of the 40 mm cylinder the typical structure observed in the case of the response function is already evident.

The method we propose for extracting the central response function from the projected data of centred cylinders is an extension of that developed in [4]. Assume that we have p circular cylinders with radii $a_1, a_2, ..., a_p$ and denote by $g_1, g_2, ..., g_p$ their projections in the CP-MCT sense. Next denote by $f_1, f_2, ..., f_p$ their projections in the Radon sense. They are given by

$$f_j(s) = 2C_j(a_j^2 - s^2)^{1/2} \tag{4.10}$$

for $|s| < a_j$, $j = 1, 2, ..., p$ and zero elsewhere. The C_j are normalization constants and the space variable s is defined in Figure 2.

Then the basic point of the method is to assume that the projections in the CP-MCT sense are given by the convolution product of the projections in the Radon sense with the unknown response function $H(s)$

$$g_j = f_j * H. \tag{4.11}$$

We point out that the response function $H(s)$ takes into account not only the incomplete path discrimination of CP-MCT (this is the effect estimated in Section 2) but also the

finite size of the receiving antenna. If we denote by $A(s)$ the aperture function of the antenna, then the relationship between the functions $K(s) = P(s, 0)$ and $H(s)$ is

$$H = A * K. \tag{4.12}$$

This relationship must be considered when comparing the theoretical results of Section 3 with those obtained from experimental data.

5. Multiple data deconvolution

The problem which must be solved is that of extracting an estimate of the response function H from the set of convolution equations

$$g_j = f_j * H + w_j, j = 1, 2, ..., p, \tag{5.13}$$

where the g_j are the CP-MCT projections of cylinder with different radii, the f_j are the corresponding Radon projections and the w_j are terms describing the contamination of the data due to noise and experimental errors. Obviously it must be assumed that all g_j, f_j are known, while the terms w_j are unknown. We point out that this identification problem is formally similar to the problem of multiple images deconvolution, investigated for instance in [9].

The most natural approach is to formulate the problem as that of determining a least-squares estimate, namely a function H minimizing the least-squares functional

$$\epsilon^2(H) = \sum_{j=1}^{p} ||f_j * H - g_j||^2. \tag{5.14}$$

Such a problem is ill-posed and therefore regularization methods must be used for its solution. Many methods are available, more or less equivalent (for a discussion see [10]), so that the choice of the particular method depends on the convenience of the user. Since in [4] we used an iterative gradient method, known as Landweber method [10], we use the same method in the present case. Such a method is not very frequently used in the applications because, in general, it requires a high number of iterations. In [4] we found that for our problem such a number is reasonable (of the order of 20-30) and therefore we do not find a reason for changing the method. In addition for such an iterative method the effect of the iterations can be easily understood.

When applied to the problem of minimizing the functional of equation (5.14) the method is as follows

$$\begin{aligned} H_0(s) &= 0 \\ H_{n+1} &= H_n + \tau \sum_{j=1}^{p} f_j * (g_j - f_j * H_n) . \end{aligned} \tag{5.15}$$

The quantity τ is a relaxation parameter satisfying the following conditions

$$0 < \tau < \frac{2}{\mid \hat{f} \mid^2_{max}}, \tag{5.16}$$

where $\mid \hat{f} \mid^2)_{max}$ denotes the maximum value of the function defined by

$$\mid \hat{f}(\omega_s) \mid^2 = \sum_{j=1}^{p} \mid \hat{f}_j(\omega_s) \mid^2 \tag{5.17}$$

the $\hat{f}_j(\omega_s)$ being the Fourier transforms of the functions $f_j(s)$.

For such a method the number of iterations plays the role of a regularization parameter in the sense that the iterates first approach the correct solution and then go away. This effect can be easily understood if one observes that the result of the n-th iteration can be written as a Fourier filter of the data [10]. Indeed, in the case of multiple deconvolution, one can prove [9] that the Fourier transform of the n-th iterate $H_n(s)$ is given by

$$\hat{H}_n(\omega_s) = [1 - (1 - \tau \mid \hat{f}(\omega_s) \mid^2)^n] \sum_{j=1}^{p} \frac{\hat{f}_j(\omega_s)\hat{g}_j(\omega_s)}{\mid \hat{f}(\omega_s) \mid^2} \tag{5.18}$$

if $\mid \hat{f}(\omega_s) \mid$ is different from zero, while $\hat{H}_n(\omega_s) = 0$ if $\mid \hat{f}(\omega_s) \mid = 0$. Therefore $H_n(s)$ is bandlimited with the same band as the CP-MCT data, as it must be. In addition if the $\hat{f}_j(\omega_s)$ have zeros inside the band and these zeros are different for different $\hat{f}_j(\omega_s)$, the simultaneous use of all f_j can compensate for the lack of information related to a single f_j; indeed, in such a case $\mid \hat{f} \mid$ is never zero inside the band. This is precisely the situation corresponding to our problem because the $\hat{f}_j$ have zeros which depend on the radius of the cylinders [4].

Since the number of iterations acts as a regularization parameter, an important issue is to find a criterion for selecting the appropriate number of iterations. The usual stopping rule is the so-called *discrepancy principle* which consists in stopping the iterations when the discrepancy $\epsilon(H_n)$ (the function $\epsilon(H)$ is defined in equation (5.14)) is of the order of the estimated rms error on the data. Unfortunately we do not have such an estimate for our data $g_j(s)$. However, if we look at the behaviour of $\epsilon(H_n)$ as a function of n, we find that it decreases very rapidly after a few iterations, up to a value of few percent and then decreases much more slowly. As a consequence of this behaviour it looks natural to stop the iterations at the beginning of the flat region. In addition we find that the result of the iterations does not change significantly in this region.

In Figure 5 we give the results obtained using 50 and 100 iterations. We see that the main effect obtained by increasing the iterations from 50 to 100 is to have a bit deeper central minimum and more pronounced side lobes. In the same figure we also give for comparison the result obtained in Section 3 (all functions are normalized in such a way

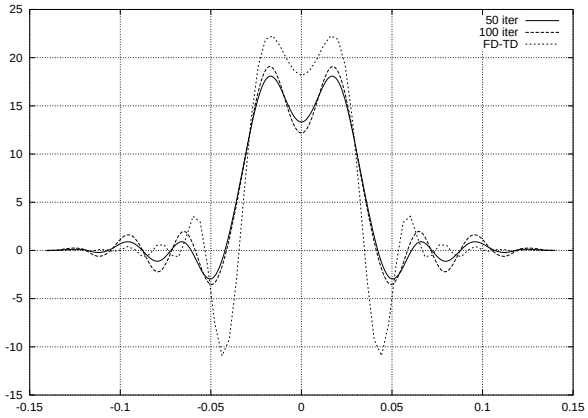

Figure 5. Response function obtained by means of multiple deconvolution: after 50 iterations (full line) and after 100 iterations (dotted line); the result is compared with that obtained in Section 3 (dash-dotted line).

that their integral is one). As it is evident the first negative side lobes of the computed response function are much deeper that those of the response function derived from the experimental data.

6. Discussion of the results

References

[1] Miyakawa M., 1993, Tomographic measurements of temperature change in the phantoms of the human body by chirp radar-type microwave computed tomography *Med Biol Eng Comput*, **31**, S31-S36

[2] Miyakawa M., 1996, Microwave imaging - 1: Microwave computed tomography, in *Non-invasive Thermometry of Human Body*, M Miyakawa and J C Bolomey eds, 105-126 (CRC Press, Boca Ranton)

[3] Jacobi J. M. and Larsen L. E., 1978, Microwave interrogation of dielectric targets. Part II: By microwave time delay spectroscopy *Med Phys*, **5**, 509-518

[4] Bertero M., Miyakawa M., Boccacci P., Conte F., Orikasa K. and Furutani M., 2000, Image restoration in chirp-pulse microwave CT (CP-MCT) IEEE *Trans Biomed Eng*, **47**, 600-609

[5] Bertero M., Conte F., Miyakawa M. and Piana M., 2000, Mathematical modeling of Chirp-Pulse Microwave Computerized Tomography (CP-MCT), submitted to Inverse Problems

[6] Furutani M., Miyakawa M., Hoshina S., Kanai Y. and Ishii N., 2000, *A numerical analysis of the tomographic imaging of the chirp radar-type micorwave computed tomography - Computation*

of the projection data based on a transfer function method, Technical Report of IEICE Japan AP98 **108** 13-18

[7] Orikasa K., Miyakawa M., and Ishii N., 2000, PSF-*based image restoration of* CP-MCT *by use of* FD-TD *method*, Technical Report of IEICE Japan MBE99 **147** 13-18

[8] Kawada Y., Miyakawa M., and Ishii N., 1999, *Generation of tomographic images of* CP-MCT *based om* FD-TD *method*, Technical Report of IEICE Japan MBE99 **82** 73-84

[9] Piana M. and Bertero M., 1996, Regularized deconvolution of multiple images of the same object, J. Opt. Soc. America, **A-13**, 1516-1523

[10] Bertero M. and Boccacci P., 1998, *Introduction to Inverse Problems in Imaging* (IOP Publishing, Bristol)